Nucleic Acids Research, 2005, Vol. 33, No. 22 ***6961–6971***
doi:10.1093/nar/gki1004

Solution structure of ψ_{32}-modified anticodon stem–loop of *Escherichia coli* tRNA^{Phe}

Javier Cabello-Villegas and Edward P. Nikonowicz*

Department of Biochemistry and Cell Biology, Rice University, Houston, TX 77251-1892, USA

Received September 13, 2005; Revised and Accepted November 17, 2005

ABSTRACT

Nucleoside base modifications can alter the structures and dynamics of RNA molecules and are important in tRNAs for maintaining translational fidelity and efficiency. The unmodified anticodon stem–loop from *Escherichia coli* tRNA^{Phe} forms a trinucleotide loop in solution, but Mg^{2+} and dimethylallyl modification of A_{37} N6 destabilize the loop-proximal base pairs and increase the mobility of the loop nucleotides. The anticodon arm has three additional modifications, ψ_{32}, ψ_{39}, and A_{37} C2-thiomethyl. We have used NMR spectroscopy to investigate the structural and dynamical effects of ψ_{32} on the anticodon stem-loop from *E.coli* tRNA^{Phe}. The ψ_{32} modification does not significantly alter the structure of the anticodon stem–loop relative to the unmodified parent molecule. The stem of the RNA molecule includes base pairs ψ_{32}-A_{38} and U_{33}–A_{37} and the base of ψ_{32} stacks between U_{33} and A_{31}. The glycosidic bond of ψ_{32} is in the *anti* configuration and is paired with A_{38} in a Watson–Crick geometry, unlike residue 32 in most crystal structures of tRNA. The ψ_{32} modification increases the melting temperature of the stem by ~3.5°C, although the ψ_{32} and U_{33} imino resonances are exchange broadened. The results suggest that ψ_{32} functions to preserve the stem integrity in the presence of additional loop modifications or after reorganization of the loop into a translationally functional conformation.

INTRODUCTION

Posttranscriptional modification of RNA molecules occurs in all cells (1–3). The modifications, which are primarily localized to the nucleotide bases, can alter the chemical, structural, and thermodynamic properties of RNAs and thereby contribute to RNA function (4). Many nucleotide base modifications have been chemically well characterized but the impact of these modifications on RNA structure and stability has been less thoroughly examined. Pseudouridine is the most common nucleotide base modification and is found in the tRNA and rRNA of all cells (5,6). This modification is formed by an isomerization of uridine resulting in a C5-C1′ base–ribose glycosidic bond and a second imino (NH) functionality. Pseudouridine preferentially adopts the *syn* conformation about the glycosidic bond as the free nucleotide (7,8), but the *anti* configuration has been most frequently observed for pseudouridine within oligonucleotides and double helices (9). Consequently pseudouridine tends to base pair with adenosine through the N3 imino and the C2 carbonyl groups (Figure 1) (10–13) and imparts thermodynamic stability to helices when located in the interior of an RNA duplex or in a single strand region adjacent to a duplex (8).

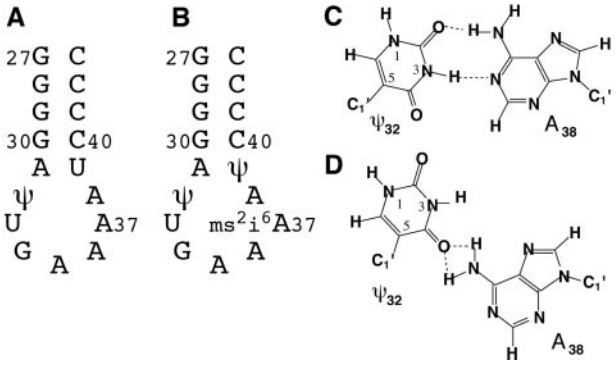

Figure 1. Sequences of (**A**) the ψ_{32}-modified and (**B**) fully modified RNA hairpins corresponding to the anticodon arm of *E.coli* tRNA^{Phe}. Nucleotide numbering corresponds to the full-length tRNA^{Phe} molecule. ψ designates pseudouridine and ms^2i^6A designates (2-thiomethyl, N6-dimethylallyl)-adenine. ψ_{32}-A_{38} base arrangements for (**C**) the Watson–Crick base pair and (**D**) the bifurcated hydrogen bond interaction.

*To whom correspondence should be addressed. Tel: +1 713 348 4912; Fax +1 713 348 5154; Email: edn@bioc.rice.edu
Present address:
Javier Cabello-Villegas, Department of Microbiology, University of Colorado Health Sciences Center, Aurora, CO 80045, USA

In addition to the nearly universally conserved ψ_{55}, pseudouridine occurs frequently at several other positions in tRNA including residues 13, 32, 39, and 40 (14), although the frequency of occurrence at these positions varies among species. ψ_{55}, located in the T-loop, serves only as an acceptor in its hydrogen bonding with the imino and amino groups of G_{18}. The ψ_{55}-G_{18} pair stacks between the flanking base pairs and contributes to maintenance of the tertiary fold of tRNA (15,16). In yeast $tRNA^{Phe}$ and other tRNAs or tRNA complexes, ψ_{39}, at the bottom of the anticodon stem, generally aligns with A_{31} in a standard A–U Watson–Crick hydrogen bond geometry (15–20), although the hydrogen bonds tend to be somewhat long (2.1–2.3 Å). ψ_{32} also is located in the anticodon arm of six tRNA species in *Escherichia coli* and adopts a *syn* configuration about its glycosidic bond in $tRNA^{Cys}$ (17). In yeast $tRNA^{Asp}$, ψ_{32} forms a bifurcated base pair with C_{38} involving ψ_{32} O4 and the exocyclic amino hydrogens of C_{38} (18,21).

Residue 32 in the anticodon arm is important for the translation function of tRNA. A central element of the extended anticodon hypothesis is that nucleotides at the stem–loop junction in the anticodon arm contribute to the translational efficiency of tRNA (22,23). The functional importance of residues 32 and 38 was first demonstrated using amber suppressor tRNAs Su2 and Su7 that incorporate glutamine and tryptophan, respectively, at the stop codon 5′-UAG-3′. These suppressor tRNAs share the same anticodon nucleotide sequence, but Su2 is a weak suppressor whereas Su7 is a strong suppressor. The different suppression efficiencies of these tRNAs originate mainly from the identities of nucleotides 32 and 38 (23). In addition to the suppressor tRNA studies of Yarus and coworkers (23), the functional significance of the 32–38 bp is further illustrated by nucleotide substitution studies of glycyl tRNAs of *E.coli* and *Mycoplasma mycoides* (24,25). The genome of *M.mycoides* encodes one $tRNA^{Gly}$ (anticodon 5′-UCC-3′) that is used to decode all four glycine codons and has a C_{32}–A_{38} mismatch in the anticodon arm. In *E.coli*, $tRNA^{Gly,2}$ has the anticodon 5′-UCC-3′, but has the base pair U_{32}–A_{38}. When mutated to a U_{32}–A_{38} base pair, the ability of the *M.mycoides* $tRNA^{Gly}$ to decode non-cognate codons dramatically diminishes (25). Similarly, mutation of the U_{32}–A_{38} base pair of *E.coli* $tRNA^{Gly,2}$ to C_{32}–A_{38} leads to decreased fidelity and −1 frameshifting at 5′-GGG-3′ codons (26). These studies demonstrate the ability of the 32–38 interaction to modulate the wobble properties of the anticodon. Thus, the types of interactions formed by residues 32 and 38 may alter the conformation and dynamics of the anticodon loop and/or the interactions within the codon-anticodon complex at the ribosome.

We have used heteronuclear NMR spectroscopy to examine the solution structure of the ψ_{32}-modified form of the anticodon arm of *E.coli* $tRNA^{Phe}$. A 17 nt RNA molecule that forms a stem–loop secondary structure in solution and corresponds to the anticodon arm of $tRNA^{Phe}$ was used (Figure 1). Our results demonstrate that the loop of the modified RNA molecule is composed of three nucleotides and lacks the characteristic U-turn motif. The anticodon arm is extended by two base pairs as in the unmodified parent molecule and ψ_{32} increases the stability of the stem. The ψ_{32} base forms a Watson–Crick type base pair with A_{38} and not the bifurcated hydrogen bond configuration found in most crystal structures of tRNAs.

MATERIALS AND METHODS

All enzymes were purchased from Sigma Chemical, except for T7 RNA polymerase and RluA enzymes, which were prepared as described (27,28). Deoxyribonuclease I type II, pyruvate kinase, adenylate kinase, and nucleotide monophosphate kinase were obtained as powders, dissolved in 15% glycerol, 1 mM dithiothreitol, and 10 mM Tris–HCl, pH 7.4, and stored at −20°C. Guanylate kinase and nuclease P1 were obtained as solutions and stored at −20°C. Unlabeled 5′ nucleoside triphosphates (5′-NTPs) were purchased from Sigma, phosphoenolpyruvate (potassium salt) was purchased from Bachem, and 99% {^{15}N}-ammonium sulfate and 99% {^{13}C}-glucose were purchased from Isotec.

Preparation of RNA samples

The RNA sequence for *E.coli* $ACSL^{Phe}$ shown in Figure 1 was synthesized *in vitro* using T7 RNA polymerase and a synthetic DNA template. The nucleotide sequence of the stem corresponds to residues G_{27}–C_{43} of full-length *E.coli* $tRNA^{Phe}$. Isotopically labeled RNA molecules were prepared from 10 ml transcription reactions using 3 mM uniformly ^{15}N-enriched and ^{13}C-enriched 5′-NTPs as described (29). The RNA molecules were purified by passage through 20% (w/v) preparative PAGE, electroeluted (Schleicher and Schuell), and precipitated with ethanol. The purified oligonucleotides were dissolved in 1.0 M NaCl, 20 mM potassium phosphate, pH 6.8, and 2.0 mM EDTA, and dialyzed extensively against 10 mM NaCl, 10 mM potassium phosphate, pH 6.8, and 0.05 mM EDTA, using a Centricon-3 concentrator (Amicon Inc.). The samples were diluted with buffer to a volume of 0.2 ml and lyophilized to a powder. For experiments involving the non-exchangeable protons, the samples were exchanged twice with 99.9% D_2O and then resuspended in 0.2 ml of 99.96% D_2O. For experiments involving detection of the exchangeable protons, the samples were resuspended in 0.2 ml of 90% H_2O/10% D_2O. The samples contained 80 and 100 A_{260} OD units of ^{15}N-labeled and ^{13}C-labeled, respectively, RNA oligonucleotides (≈2.5–3.4 mM).

Preparation of the ψ_{32}-$ACSL^{Phe}$

Pseudouridine was introduced at position U_{32} of purified $ACSL^{Phe}$ using the pseudouridine synthase RluA (RluA). Histidine-tagged RluA was expressed in *E.coli* and purified using Ni^{2+} affinity resin as described (28). The pseudouridylation reaction was carried out using a mole ratio of RluA:RNA of 1:48. The reaction conditions were 50 mM HEPES pH 7.5, 100 mM NH_4Cl, 0.03 mg/ml RluA, 0.06 mM $ACSL^{Phe}$. The reactions were allowed to proceed overnight at 37°C. The RNA was purified from the RluA enzyme by heating the reaction to 90°C for 2 min followed by centrifugation to remove the precipitated protein. The supernatant was dialyzed with NMR buffer. Completion was determined by the disappearance of the C5–H5 resonance of U_{32} from 2D ^{13}C-^{1}H HMQC spectra (Supplementary Figure S1). The reactions could not be monitored using denaturing PAGE because the modified $ACSL^{Phe}$ migrates at the same rate as the unmodified $ACSL^{Phe}$.

NMR spectroscopy

All NMR spectra were acquired on a Bruker AMX-500 spectrometer equipped with a ^{1}H-{X} broadband probe, except for

the ^{31}P-decoupled ^{13}C-^{1}H constant time HSQC experiment, which was collected with a ^{1}H-{^{13}C, ^{31}P} triple resonance probe. Broadband decoupling of the carbon and nitrogen resonances was achieved using GARP with $\gamma B_2 = 3125$ Hz for carbon and $\gamma B_2 = 1570$ Hz for nitrogen. H_2O spectra were collected at 12°C with solvent suppression using either spin lock pulses or binomial read pulses with maximum excitation at 12.5 p.p.m. D_2O spectra were collected at 25°C with presaturation or spin lock pulses to suppress the residual HDO peak. Quadrature detection was achieved using the States-TPPI method, and acquisition was delayed by a half-dwell in all indirectly detected dimensions. Typically, the data points were extended by 25% using linear prediction for the indirectly detected dimensions and the data were apodized using 1 Hz line broadening and 65° shifted sinebell functions. ^{1}H spectra were referenced relative to DSS (0.00 p.p.m.). References for the ^{13}C and ^{15}N spectra were calculated using the spectrometer frequencies as reported (30). The ^{31}P spectra were referenced to an external standard of TMP which was set at 0.00 p.p.m. All spectra were processed and analyzed with Felix 98.0 (Accelerys, Inc.).

2D ^{13}C-^{1}H HMQC and HSQC spectra were collected to identify ^{13}C-^{1}H chemical shift correlations. 2D HCCH-COSY and 3D HCCH-TOCSY (24 ms DIPSI-3 spin lock) experiments optimized for polarization transfer through the ribose carbons and a 2D ^{13}C-^{1}H HCCH-TOCSY (52 ms DIPSI-3 spin lock) optimized for polarization transfer through the adenine bases were collected in D_2O to identify ribose spin systems and H8-H2 correlations, respectively (31,32). To identify intra-residue base-sugar correlations, a 2D ^{15}N-^{1}H HSQC experiment was acquired in D_2O and optimized for two- and three-bond correlations. A J(N, N)-HNN COSY experiment was acquired in D_2O to confirm the presence of A•U base pairs (33) and ^{31}P assignments were obtained using a ^{31}P/^{1}H hetero-TOCSY-NOESY spectrum (34).

Distance constraints for the non-exchangeable resonances of ψ_{32}-modified ACSL^{Phe} were derived at 25°C from 2D ^{1}H-^{1}H NOESY spectra (80, 120, 180, 360, and 480 ms mixing times), ^{13}C-edited 3D NOESY-HMQC spectra (180 and 360 ms mixing times), and ^{13}C-edited 3D NOESY-ctHSQC spectra (80, 180, and 360 ms mixing times) optimized for the ribose resonances in ω_2 and ω_3. For the exchangeable resonances, 2D ^{15}N-^{1}H HSQC spectra were collected to identify ^{15}N-^{1}H chemical shift correlations. 2D ^{1}H-^{1}H NOESY experiments optimized for imino (NH) proton resonances were acquired at 60 and 360 ms mixing time in 90% H_2O to obtain distance restraints involving the exchangeable protons.

Backbone torsion angle constraints were derived from ^{1}H-^{1}H and ^{31}P-^{1}H coupling constants obtained from the following experiments. A ^{31}P-decoupled DQF-COSY experiment and a 2D ^{31}P-^{1}H HetCor experiment were acquired in D_2O with unlabeled RNA samples.

Interproton distance constraints

Semi-quantitative distance constraints between non-exchangeable protons were estimated from cross peak intensities in 2D NOESY and 3D ^{13}C-edited NOESY spectra. Using the covalently fixed pyrimidine H5-H6 distance (≈2.4 Å) and the conformationally restricted sugar H1′-H2′ distance (2.8–3.0 Å) as references, peak intensities were classified as strong, medium, weak, or very weak and their corresponding proton pairs given upper bound distance constraints of 3.0, 4.0, 5.0, or 6.0 Å, respectively. Cross peaks observed only at mixing times >180 ms were classified as extremely weak and given 7.0 Å upper bound distance constraints to account for the possibility of spin diffusion. All distance constraints were given lower bounds of 1.8 Å. Distance constraints involving exchangeable protons were estimated from 360 ms mixing time NOESY spectra and were classified as either weak, very weak, or extremely weak, except for the intra-base pair distances A•U H2–NH and G•C NH–NH_2, which were classified as strong constraints. Only intra-residue sugar-to-sugar constraints involving H5′ and H5″ resonances were included in the calculations.

An initial set of structures was calculated using a shortened version of the simulated annealing protocol (described below). A list of all proton pairs in the calculated structures closer than 4.0 Å (representing expected NOEs) was compared to the list of constraints. The NOESY spectra were then re-examined for predicted NOEs absent from the constraint list. In some cases, this allowed the unambiguous assignment of previously unidentified NOEs, but, in other cases, the predicted NOEs were unobservable due to spectral overlap or the broadening of resonances by exchange with solvent. After the final calculations, virtually all predicted NOEs not in the list could be accounted for by spectral overlap or exchange broadening.

Hydrogen bonding constraints

Watson–Crick base pairs were identified using two criteria: the observation of a significantly downfield shifted NH or NH_2 proton resonance and the observation of strong G•C NH–NH_2 or A•U H2–NH NOEs. The A_{37}•U_{33} base pair was identified by observation of a cross peak between A_{37}H2 and U_{33}N3 in the J(N, N)-HNN COSY spectrum. Hydrogen bonds were introduced as distance restraints of 2.9 ± 0.3 Å between donor and acceptor heavy atoms and 2.0 ± 0.2 Å between acceptor and hydrogen atoms. Constraints identified in this way were included in the calculations for base pairs G_{27}•C_{43}, G_{28}•C_{42}, G_{29}•C_{41}, G_{30}•C_{40}, A_{31}•U_{39}, and ψ_{32}•A_{38}. The U_{33}•A_{37} base pair constraint was set to 2.9 ± 1.2 Å and 2.0 ± 1.2 Å between donor and acceptor heavy atoms and acceptor and hydrogen atoms, respectively, to permit conformational freedom of loop residues.

Dihedral angle constraints

Constraints on the ribose ring and backbone dihedral angles were derived from semi-quantitative measurements of $^{3}J_{H\text{-}H}$ and $^{3}J_{H\text{-}P}$ couplings (35,36). Sugar pucker conformations were determined from $^{3}J_{H1'\text{-}H2'}$ couplings in ^{31}P-decoupled 2D DQF-COSY spectra. Residues with H1′-H2′ couplings >7 Hz were constrained to the C2′-endo conformation through two of the torsion angles in the ribose sugar ring (37). Independent confirmation of sugar pucker conformation was provided by the observation of weak (<5 Hz) $^{3}J_{H3'\text{-}H4'}$ couplings, C3′ resonances shifted downfield to 76–80 p.p.m. from the main cluster at 70–72 p.p.m., and C4′ resonances shifted downfield to 85–86 p.p.m. from the main cluster at 82–84 p.p.m. Residues with weak (<5 Hz) $^{3}J_{H1'\text{-}H2'}$ couplings were constrained to the C3′-endo conformation. Residues with intermediate $^{3}J_{H1'\text{-}H2'}$

couplings were left unconstrained to reflect the possibility of conformational averaging.

Dihedral angle constraints for the γ torsion angle were derived from $^3J_{H4'-H5'}$ and $^3J_{H4'-H5''}$ couplings in the DQF-COSY spectrum and intra-residue H4′-H5′ and H4′-H5″ cross peak intensities in the 80 ms mixing time 3D NOESY-ctHSQC spectrum. For residues in which H4′-H5′ and H4′-H5″ peaks in the DQF-COSY spectra were clearly absent, representing couplings <5 Hz, γ was constrained to the *gauche*$^+$ conformation (60 ± 20) (35,36). For residues with clear $^3J_{H4'-H5'}$ or $^3J_{H4'-H5''}$ couplings >5 Hz and unequal H4′-H5′ and H4′-H5″ NOE intensities, γ was constrained to include both the *trans* and gauche$^-$ conformations (−120 ± 120), reflecting the lack of stereospecific assignments for the H5′ and H5″ resonances. For residues with only weak or unobservable $^3J_{H4'-H5'}$ or $^3J_{H4'-H5''}$ couplings and unequal H4′-H5′ and H4′-H5″ NOE intensities, γ was left unconstrained to reflect the possibility of conformational averaging.

Dihedral angle restraints for the β torsion angles were derived from $^3J_{P-H5'}$ and $^3J_{P-H5''}$ couplings measured in 2D ^{31}P-^{1}H HetCor spectra. β was constrained to the *trans* conformation (180 ± 40) for residues in which P-H5′ and P-H5″ peaks in the HetCor spectra were clearly absent, representing couplings <5 Hz (35,36). For residues in which P-H5′ and P-H5″ peaks could be observed, β was left unconstrained to reflect the lack of stereospecific assignments and the possibility of conformational averaging. All P-H3′ couplings that could be clearly identified were >5 Hz which allows for both *trans* and *gauche*- conformations for the ε torsional angle. A refinement that constrained ε angles in the stem (G27-C43 to A31-U39) to −125 ± 80 had small improvements (relative to not constraining ε) on the quality of the stem regions of the structures and were therefore included for the structures reported here.

Dihedral angle restraints for α and ζ were derived from the observation that a *trans* conformation of either dihedral angle is generally associated with a large downfield shift of the bridging ^{31}P resonance (38). Because no such shift is observed for any of the ^{31}P resonances in the RNA molecules, α and ζ were loosely constrained to exclude the *trans* conformation (0 ± 120) for all residues except those in the loop regions (nucleotides U_{33} to A_{37}), which were left unconstrained. No dihedral angle constraints were used for the glycosidic angle χ. A total of 48 restraints (11 α, 8 β, 9 γ, 9ε, and 11 ζ) were used constrain the phosphate backbone dihedral angles in the calculations.

Structure calculations

All calculations were carried out on Silicon Graphics O_2 work stations using X-PLOR 3.851 (39). The dihedral angles of a linear starting structure (generated using Insight II, Molecular Simulations, Inc.) were randomized to generate 75 structures with randomized coordinates which were used in a simulated annealing/restrained molecular dynamics (rMD) routine (36,37). The calculation protocol was divided into three stages: global fold, refinement, and final minimization. The global fold step consisted of 1000 cycles of unconstrained energy minimization, 10 ps of rMD at 1000 K using only hydrogen bond and NOE constraints, 9 ps of rMD at 1000 K during which repulsive van der Waals forces were introduced, 14 ps of rMD while cooling to 300 K, and 1000 cycles of constrained minimization. The structures were then refined with 500 cycles of constrained minimization, 5 ps of rMD at 1200 K during which the α, β, γ, ε, ζ, and sugar ring dihedral constraints were slowly introduced followed by 5 ps of rMD while cooling to 300 K, and 1000 cycles of constrained minimization. The final minimization step consisted of 1000 cycles of conjugate gradient energy minimization using all constraints and repulsive van der Waals potentials. To determine the consistency of the NMR data with the tri-loop conformation of the unmodified anticodon stem–loop, an additional set of calculations was performed using constraints involving overlapped resonances that were derived from spectra of the unmodified RNA molecule. These calculations were performed beginning with the coordinates of converged structures from the global-fold rMD simulation. Structures were viewed using Insight II (Accelerys, Inc.). The structure coordinates have been deposited in the rcsb with accession number 2AWQ.

Thermal stability

UV melting studies were performed using 2.2 μM RNA hairpin dissolved in NMR buffer (10 mM NaCl, 10 mM potassium phosphate, pH 6.8, and 0.05 mM EDTA). The samples were heated to 90°C for two minutes and snap cooled on ice before each melt experiment. A_{260} absorbance spectra from 20–95°C and from 95–20°C were acquired (1.0°C per minute) on a Pharmacia Ultrospec 2000 UV-Visible spectrophotometer equipped with a peltier melting heating apparatus. The melting curves were acquired in triplicate but could not be fit to a two-state model.

RESULTS

Effect of ψ_{32} modification on RNA stability

The thermal stability of the ACSL^{Phe} and ψ_{32} ACSL^{Phe} RNA hairpins (Figure 1) was investigated using UV melting experiments to determine overall molecular stability (T_m). The UV thermal denaturation curves indicate that the hairpins melt in two stages (Figure 2). The lower temperature (<50°C) transitions presumably correspond to the destacking of the loop

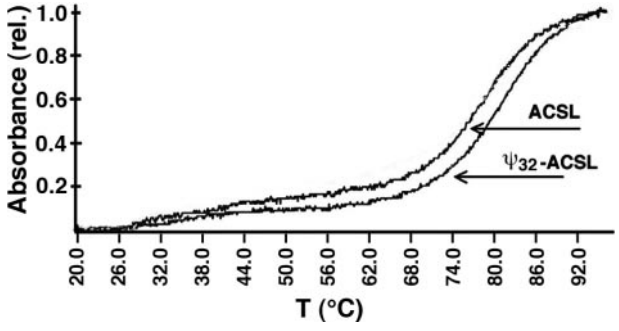

Figure 2. Overlay of the UV melting curves of the unmodified (ACSL) and ψ_{32}–modified RNA (ψ_{32}-ACSL) hairpins. Each of the hairpins appears to exhibit two melting transitions—the broad lower temperature transitions presumably corresponding to destacking of the loop nucleotide bases. The apparent melting temperatures of the unmodified and ψ_{32}–modified RNA hairpins are estimated to be 77.0°C and 73.5°C, respectively.

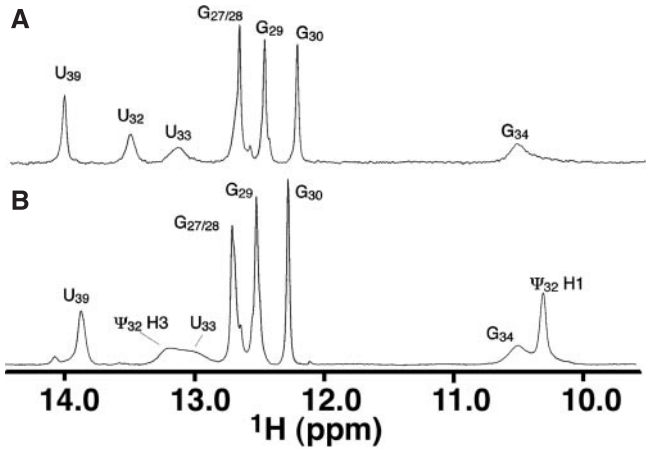

Figure 3. Imino proton spectra of the (**A**) unmodified and (**B**) ψ_{32}-modified ACSL^{Phe}. The imino resonances of ψ_{32} and U_{33} have chemical shifts consistent with Watson–Crick base pairs but are exchange broadened in ψ_{32}-ACSL^{Phe}. This suggests that the pseudouridine has a small destabilizing effect on the loop leading to increased solvent exposure of the imino groups.

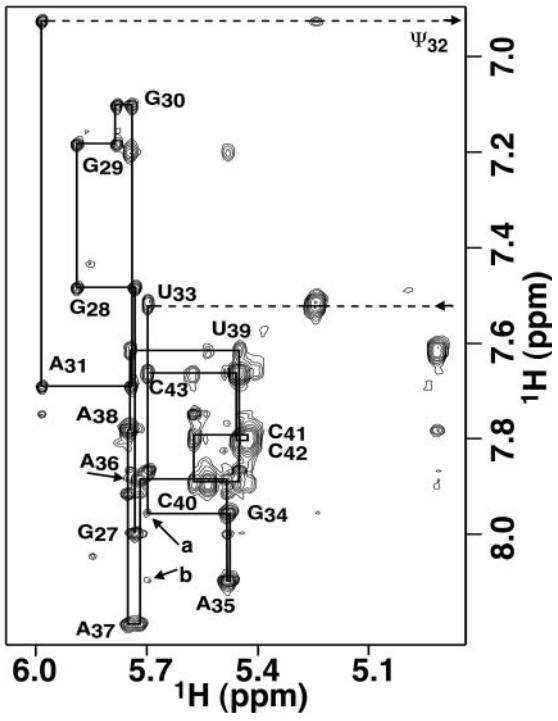

Figure 4. H6/8-to-H1′ region of the 2D 400 ms NOESY spectrum. The base-1′ proton sequential walk is traced with intra-residue peaks labeled. The ψ_{32} H1′ resonance has a chemical shift of 4.56 p.p.m. and is data not shown. The arrows (a) points to the inter-residue sequential NOE between U_{33} H1′ and G_{34} H8 and (b) non-sequential NOE between U_{33} H1′ and A_{35} H8. The presence of the sequential NOE is not compatible with a U-turn motif for the loop whereas the non-sequential NOE can be produced by non-U-turn loop conformations.

nucleotides. The pseudouridine modification shifts the transition midpoint for the hairpin 3.5°C ± 0.5°C higher. This indicates that ψ_{32} increases the stability of the stem. The anneal spectra from 95–20°C also were acquired and showed 1.2°C ± 0.5°C of hysteresis at the T_m. Slow cooling of the RNA can lead to duplex formation and to hysteresis. The increased thermal stability of the modified RNA hairpin is consistent with other studies that predict pseudouridine enhances stability when located in a stem or at a loop–stem junction (8,9). Increased stability of the upper stem and slightly lower stability of the loop is supported by the NH spectrum (Figure 3). The guanine NH protons sharpen with the introduction of ψ_{32} and the U_{33} resonance is broadened.

Resonance assignments of ψ_{32}-ACSL^{Phe}

The non-exchangeable ^{1}H and ^{13}C resonances of ψ_{32}-ACSL^{Phe} were assigned using standard heteronuclear methods (31,40). Most of the base and ribose ^{1}H-^{13}C correlations are resolved, and none of the resonances have spectral characteristics indicative of intermediate exchange. All 17 ribose spin systems, except for the incompletely labeled 5′-terminal nucleotide, were identified using 2D HCCH-COSY and 3D HCCH-TOCSY experiments. The five adenine intra-base H8-H2 correlations also were identified using the HCCH-TOCSY experiment. Intra-residue base-to-sugar correlations were identified using 2D ^{15}N-^{1}H HSQC experiments optimized to yield the multiple bond correlations H5/6-N1, H8-N9, and H1′-N1/N9 (41). All purine correlations and four of six pyrimidine correlations were identified in these spectra.

Sequence specific assignments were determined using two-dimensional (2D) NOESY (Figure 4) and 3D ^{13}C-edited NOESY experiments (31). The sequential base-1′ NOE connectivities are continuous through all 17 nt in the 180 ms NOESY spectrum, but the connectivity between nucleotides U_{33} and G_{34} is weak. With the exception of the A_{35} H8 to A_{36} H8 step, the base-2′ and base–base inter-residue connectivities also are continuous in the 180 ms spectrum. Additionally, the base-2′ inter-residue connectivities from U_{32} to A_{37} are weak, consistent with the non-C3′-endo ribose ring conformations of these residues (described below).

The exchangeable NH and NH_2 resonances were assigned using 2D NOESY experiments. The NH proton spectrum is shown in Figure 3. The three strong G NH resonances corresponding to G•C base pairs and one U NH resonance corresponding to an A•U base pair are connected by NOE cross peaks between NH proton resonances of adjacent base pairs. These connectivities are continuous in the helix from G_{28} to U_{39}. The weak NH resonance of the terminal G•C base pair does not yield cross peaks in the NOESY spectrum. The U_{33} NH resonance is weak (Figure 3) and could only be assigned through a U_{33} N3–A_{37} H2 cross peak in the J(N, N)-HNN COSY spectrum (Figure 5) (33). A weak G NH resonance, which has a chemical shift that corresponds to a non-base paired guanine, was assigned to G_{34}. The cytidine NH_2 resonances were assigned using the strong intra-base pair C NH_2 to G NH NOE cross peaks. The NH_2 resonances of A_{37} and of all guanine nucleotides except G_{34} were not observed. The A_{31} NH_2 resonances were assigned based on their NOE cross peaks with U_{39} H3. The NH_2 ^{15}N resonances of A_{35}, A_{36} and A_{38} were assigned based on intrabase H2 to N6 correlations in the J(N, N)-HNN COSY spectrum. The NH_2 proton resonances of A_{35} and A_{36} are broad and have chemical shifts indicative of solvent-exposed protons.

Resonance assignments for ψ_{32} were accomplished using conventional heteronuclear methods. The ψ_{32} C1′ resonance is shifted upfield into the region of the C4′ resonances at

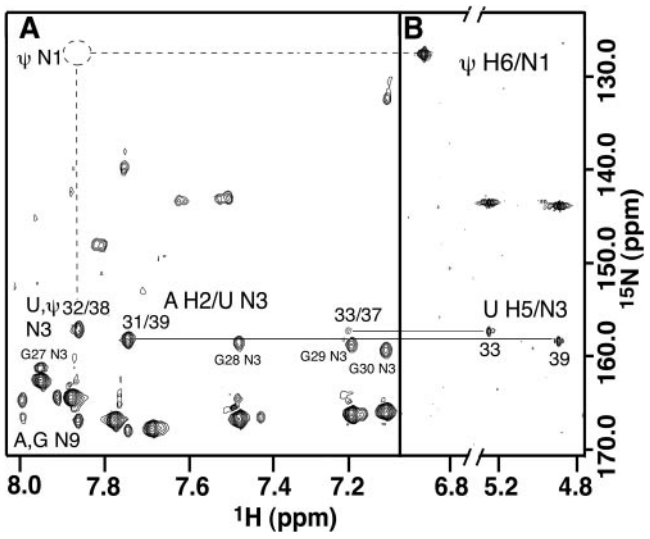

Figure 5. (**A**) HNN-COSY and (**B**) multiple-bond ^{15}N-^{1}H HSQC spectra showing intra-residue U H5 to N3 and ψ H6 to N1 correlations. The HNN-COSY shows cross-strand H2-N3 crosspeaks for residues 31–39, 38–32, and 37–33 produced by the Watson–Crick base pair configurations. The *syn* configuration about the ψ_{32} glycosidic bond and participation of ψ_{32} N1H in the ψ_{32}-A_{38} base pair would produce a ψ_{32} N1-A_{38} H2 crosspeak (dashed circle). The U_{33}–A_{37} crosspeak is weak and is indicative of a weak hydrogen bond.

82.78 p.p.m. This position is consistent with the carbon–carbon glycosidic bond that replaces the more electronegative nitrogen–carbon bond of uridine. The ψ_{32} H6 has a sequential NOE cross peak with A_{31} H1′ and the ψ_{32} H1′ has a cross peak with the U_{33} H6. The ψ_{32} H1′ assignment was confirmed through direct correlation with the ψ_{32} H6 using an HCCH-RELAY experiment. The ψ_{32} H1 and N1 imino resonances give rise to a cross peak in the 2D ^{15}N-^{1}H HMQC spectrum at 10.31 (^{1}H) and 128.59 (^{15}N) p.p.m. The identity of the N1 imino resonance is confirmed by the two-bond correlation with H6 in the multiple-bond HSQC spectrum (Figure 5). An intense intrabase NOE crosspeak between the N1H and H6 of ψ_{32} also supports assignment of the ψ_{32} H1. The ψ_{32} N3H resonance was assigned based on its NOE cross peak with the A_{38} H2 since the ψ_{32} H3 resonance is weak and does not give rise to a cross peak with the U_{39} NH resonance.

All of the internucleotide phosphate ^{31}P resonances are clustered between −3.35 and −4.63 p.p.m. and were assigned using a ^{31}P-^{1}H hetero-TOCSY-NOESY experiment. The sequential P–H6/8 and P–H1′ correlations are continuous throughout the molecule. The P–H3′ correlations and several P–H4′ and P–H5′/H5″ correlations are present in ^{31}P–^{1}H HetCor spectra and provide independent confirmation of the ^{31}P assignments. The 5′ terminal phosphate resonates at −1.30 p.p.m. and was assigned through cross peaks to the ribose protons of G_{27}.

Structure calculations

The structure of ψ_{32}-ACSL^{Phe} was calculated using a rMD routine starting from 75 sets of coordinates with randomized backbone dihedral angles. The calculations used a total of 238 NOE derived distance constraints, 36 bp constraints, and 74 dihedral angle constraints (Table 1) resulting in 10 converged structures (Figure 6). Structures were classified as converged if they had low energy, few constraint violations, and predicted only NOEs that could be experimentally verified or explained. The converged structures have an average of 5 distance constraint violations between 0.1 and 0.3 Å, most of these involving the loop region. All converged structures have no constraints violated by more than 0.3 Å. The average root mean square deviations (RMSDs) of the heavy atoms between the individual structures and the minimized mean structure is 0.67 Å for the loop region (residues 33–37) and 0.92 Å for the stem region (residues 27–32 and 38–43) (Figure 6).

Table 1. Summary of experimental constraints and structure calculation statistics for ψ_{32}-ACSL^{Phe}

Constraint	
NOE distance constraints	
Intraresidue[a]	88
Interresidue	150
Mean number per residue	14.0
NOE constraints by category	
Very strong (1.8–3.0 Å)	7
Strong (1.8–4.0 Å)	24
Medium (1.8–5.0 Å)	70
Weak (1.8–6.0 Å)	88
Very weak (1.8–7.0 Å)	49
Base pair constraints	
Total[b]	36
Dihedral angle constraints	
Ribose ring[c]	26
Backbone	48
Mean number per residue	4.3
Violations	
Average distance constraints > 0.3Å[d]	0
RMSDs for distance constraints (Å)	0.027
Average dihedral constraints > 0.5[e]	3.7
RMSDs for dihedral constraints (°)	0.26
RMSD from ideal geometry[f]	
Bonds (Å)	0.006
Angles (°)	1.4

[a]Only conformationally restrictive constraints are included.
[b]The number of base pair constraints includes U_{33}•A_{37} base pair constraints.
[c]Three torsion angles within each ribose ring were used to constrain the ring to either the C2′-endo or C3′-endo conformation. The ring pucker of residues U_{33} and A_{37} were not constrained.
[d]A distance violation of 0.3 Å corresponds to 5.0 kcal energy penalty.
[e]A dihedral angle violation of 0.5° corresponds to 0.05 kcal energy penalty.
[f]Calculated for the minimized average structure.

Structure of the loop region of ψ_{32}-ACSL^{Phe}

The ψ_{32}-ACSL^{Phe} loop is made up of the anticodon nucleotides G_{34}–A_{36} and is closed by the U_{33}•A_{37} base pair (Figure 7). The base of G_{34} stacks against the base of U_{33}, consistent with the observed H6-H8 and H5-H8 NOEs. The bases of G_{34} and A_{35} are approximately coplanar and are parallel. This configuration satisfies the observed G_{34} H8–A_{35} H8 NOE cross-peak. The A_{36} base stacks beneath A_{37} base but is displaced toward the minor groove edge of A_{37} (Figure 7). Several NOEs involving the A_{36} H2 resonance help position this base and include interactions with the H2′ of U_{33}, the H8 of A_{35}, and the G_{34} and/or A_{35} H1′ (these 1′ resonances are degenerate). These cross-peaks indicate that the Watson–Crick base pair functional groups are oriented to the interior of the molecule and point toward the residues

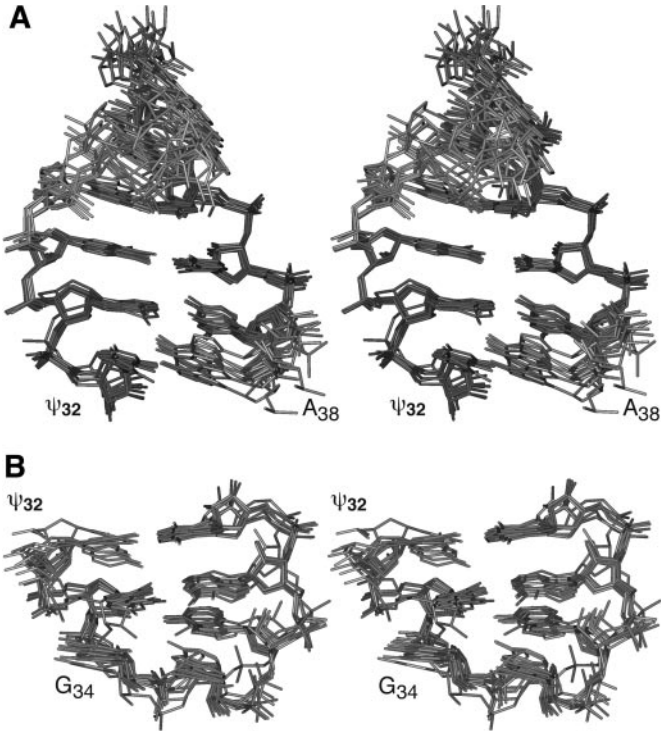

Figure 6. Stereoview of the superposition of (**A**) the stems and (**B**) the loops of the 10 converged ψ_{32}-ACSL^{Phe} structures. Convergence criteria are given in the text. The views are into the major groove. Only sugar and base heavy atoms are shown and the average r.m.s. deviation for the heavy atoms between the ten structures and the average structure is 1.14 Å. The loop and stem regions are locally well defined, but the propeller twist of the A_{31}–U_{39} base pair is variable among the structures and slightly increases the r.m.s.d. of the full hairpin.

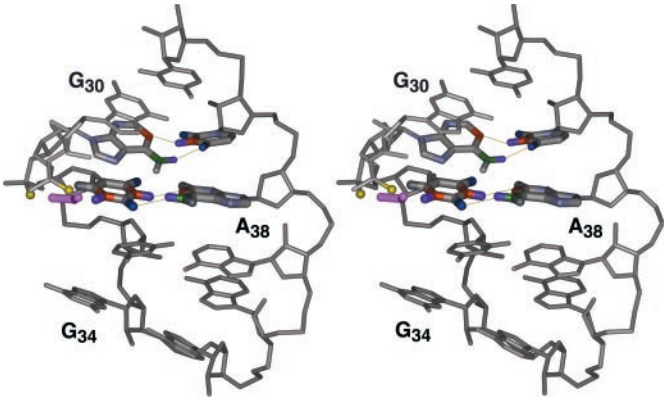

Figure 7. Stereoview of minimized average structure of ψ_{32}-ACSL^{Phe} (residues G_{30} to C_{40}). Hydrogen bonding NH and NH_2 protons of base pairs ψ_{32}-A_{38} and A_{31}–U_{39} are colored purple and the exocyclic amino nitrogens (A_{31} and A_{38}) are green. The pro-R(p) phosphoryl oxygens of A_{31} and ψ_{32} (yellow) are predicted to form water-mediated hydrogen bonds with ψ_{32} N1H and slow exchange of the N1 proton. The bridging water molecule is shown in pink. Explicit waters were not used for the structure calculations, but upper distance bounds derived from crystal structures were applied between ψ_{32} N1 and the phosphoryl oxygens.

flanking the 5′ side of the nucleotide. The conserved NOE cross-peaks A_{36} H2 to A_{37} H2 and H1′ suggest that A_{36} is partially stacked with A_{37}. Thus, the observed NOEs support the compact tri-loop conformation.

The loop nucleotides also have unusual sugar–phosphate backbone conformations The large H1′–H2′ couplings of residues G_{34}–A_{36} indicate that the ribose sugar rings have the C2′-endo conformation. The strong intra-residue and weak sequential H2′ to H8 NOE cross-peaks as well as the substantial downfield shift of the C3′ and C4′ resonances involving residues G_{34}–A_{36} also support the C2′-endo conformation. Residues U_{33} and A_{37} at the junction of the loop and stem have a mixture of C2′- and C3′-endo conformations as evidenced by their intermediate H1′–H2′ couplings and the modest downfield chemical shifts of their C3′ and C4′ resonances. The ε torsion angles of A_{35} and A_{36} have the *-gauche* conformation not typical of A-form geometry.

A superposition of the loop regions from the ten converged structures is shown in Figure 6B and the minimized average structure is shown in Figure 7. The helical base stack is continuous along the 3′ side of the loop, with G_{34} stacking against the U_{33} base. On the 3′ side of the loop, the A_{37} base straddles the bases of A_{35} and A_{36}. The A_{36} N6 is 3 Å from the U_{33} O2′ in half of the converged structures, suggesting the possibility of a cross strand base–sugar hydrogen bond. However, this interaction could not be confirmed since the A_{36} NH_2 proton resonances could not be assigned and no 2′-OH proton resonances were identified.

The loop of the ψ_{32}-ACSL^{Phe} does not contain the classical 'U-turn' motif. Although weak, the inter-residue U_{33} H1′–G_{34} H8 and U_{33} H6–G_{34} H8 NOE cross-peaks (Figure 4) are consistent with the U_{33} and G_{34} positions shown in Figure 7 but not with their positions in the U-turn (Figures 8B and C). A U_{33} H1′ to A_{35} H8 NOE is observed, but only at long mixing time and is even less intense than the sequential U_{33} H1′–G_{34} NOE (Figure 4). The ribose puckers of the anticodon nucleotides of the U-turn also tend toward the C3′-endo conformation rather than the C2′-endo conformation observed in this study. Another feature characteristic of the U-turn motif is the *trans* conformation of backbone torsion angle α between U_{33} and G_{34}. The ^{31}P resonance corresponding to this phosphate is located in the main cluster of ^{31}P peaks (Supplementary Table S1). The chemical shift of this resonance is not consistent with the ^{31}P chemical shift predicted for a phosphate having the *trans* conformation of the α torsional angle (38).

Structure of the stem of ψ_{32}-ACSL^{Phe}

The geometry of the hairpin stem, base pairs G_{27}•C_{43} to U_{33}•A_{37}, is primarily A-form (Figure 6A). The sequential base-1′, 2′ and several base–base NOEs are continuous at 180 ms mixing time. The A_{31}•U_{39} and ψ_{32}•A_{38} base pairs are sufficiently stable to give rise to a cross-strand NH–H2 NOEs, but the NH proton of the U_{33}•A_{37} base pair is not. The ψ_{32} and U_{33} NH proton resonances are weak, but their participation in Watson–Crick pairing schemes was confirmed using a J(N, N)-HNN-COSY spectrum (Figure 5). Nucleotides A_{31}, A_{37}, and A_{38} also produce cross-strand H2-H1′ NOEs commonly observed for A•U base pairs within helices. The H2 to N3 through bond correlations clearly confirm that U_{39} is base paired with A_{31} and ψ_{32} is base paired with A_{38} through its N3 imino group (Figure 7).

The torsion angles of the sugar-phosphate backbone are within the limits of A-form geometry. The small (<5 Hz) H1′–H2′ couplings and the ^{13}C chemical shifts of the 3′ and

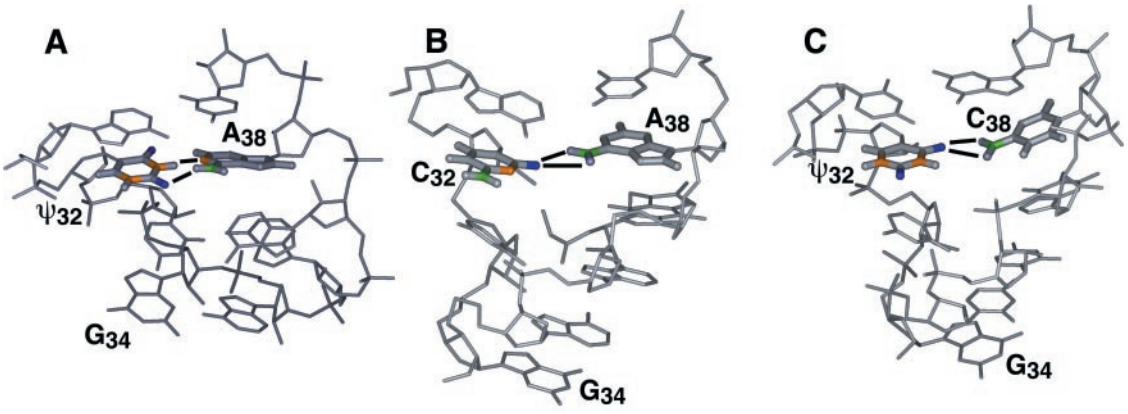

Figure 8. Comparison of residues 31–39 of (**A**) the solution structure of *E.coli* $tRNA^{Phe}$ (42) and the crystal structures of (**B**) fully modified yeast $tRNA^{Phe}$ (15,16) and (**C**) fully modified $tRNA^{Asp}$ (18,21). ψ_{32} and A_{38} in (A) form a Watson–Crick base pair. In (B) and (C), nucleotides C_{32}-A_{38} and ψ_{32}-C_{38}, respectively, form the bifurcated hydrogen bond. The anticodon loop in (A) adopts the tri-loop conformation whereas the anticodon loops in (B) and (C) adopt the U-turn motif. In *E.coli* $tRNA_{Cys}$, ψ_{32} is in the *syn* configuration about the glycosidic bond and the loop forms a U-turn motif (17).

4′ resonances of nucleotides G_{28}–ψ_{32} and A_{38}–C_{42} are indicative of the typical C3′–endo sugar pucker. None of the α or ζ torsional angles within the converged structures deviated from gauche$^-$.

The most remarkable feature of the stem is the minimal structural perturbation caused by ψ_{32}. Although the combination of A_{31} H8-ψ_{32} H6 and A_{31} H2-ψ_{32} H6 NOEs is unusual, the relative positions of the adjacent A_{31} and ψ_{32} bases that give rise to the interactions are accommodated within the A-form helix.

DISCUSSION

We are using the anticodon stem–loop of *E.coli* $tRNA^{Phe}$ as a model to probe the cumulative physical effects of sequential modifications in RNA molecules. Pseudouridine is the most common base modification found in RNA and the anticodon stem-loop of *E.coli* $tRNA^{Phe}$ has two of these nucleotides, ψ_{32} and ψ_{39}. In this study, we have examined the thermodynamic and structural effects of ψ_{32} on the otherwise unmodified $tRNA^{Phe}$ anticodon stem–loop.

The structures of $ACSL^{Phe}$ and ψ_{32}-$ACSL^{Phe}$ are similar

The unmodified anticodon stem–loop of $ACSL^{Phe}$ forms a highly ordered tri-loop conformation (42) and the ψ_{32}-$ACSL^{Phe}$ adopts a similar structure. The stems of the two hairpins are continuous through base pair U_{33}–A_{37}, but this loop-closing base pair is weaker in the ψ_{32}-modified molecule indicating a slightly less compact tri-loop. Also, fewer constraints involving G_{34} and A_{35} in ψ_{32}-$ACSL^{Phe}$ lead to greater variability in the positions of these residues compared to the unmodified molecule, including excursions of A_{35} to the minor groove side of the loop. However, the lower number of experimental constraints in the loop is due to spectral overlap of G_{34} and A_{35} H1′ resonances and probably does not reflect conformational heterogeneity inherent in the loop. Nonetheless, the small chemical shift differences between unmodified and ψ_{32}-modified $ACSL^{Phe}$ molecules indicate that the loop structures are not identical. The energy difference between the converged conformations of ψ_{32}-$ACSL^{Phe}$ is small (<15 kcal/mole), and the RMSD between the ψ_{32}-$ACSL^{Phe}$ and $ACSL^{Phe}$ minimized average structures is 1.13 Å.

The pseudouridylation of U_{32} increases the overall stability of the RNA hairpin. This is consistent with studies that have examined the thermodynamic effects of pseudouridine incorporation (9,13,43,44). Pseudouridine within a helix can increase the melting temperature of the helix 3–5°C depending upon the neighboring base pairs and improves local base stacking (9). A contributing factor to the stabilization effect of ψ is its ability to form a water-mediated hydrogen bond with the phosphate backbone (9). This hydrogen bond interaction has been inferred from difference maps of X-ray crystallographic studies of unmodified and fully modified $tRNA^{Gln}$ molecules (19) and is present in molecular dynamics simulations of yeast $tRNA^{Asp}$ (45). The strong exchange-protected ψ_{32} N1H resonance (Figure 3) supports this interaction within the $ACSL^{Phe}$ and is modeled in the average structure (Figure 7). Pseudouridine also confers a smaller degree of helix stabilization when present in single strand regions adjacent to a helix (46) or is on the 3′ end of the loop at loop-helix junctions such as ψ_{39} (46). ψ_{32} is adjacent to the helix-loop junction (U_{33}–A_{37}), but is at the 5′ end of the loop. Thus, pseudouridine has a comparable stabilizing effect when positioned on either the 3′ or 5′ edge of a helix.

Pseudouridine tends to form a Watson–Crick base pair with adenine in helical contexts and the ψ_{32} is no exception (43). The HNN-COSY spectrum confirms the hydrogen bond configurations of the ψ_{32}-A_{38} and U_{33}–A_{37} base pairs (Figure 5). However, the H3 resonances of U_{33} and ψ_{32} are weaker than the corresponding H3 resonances of unmodified $ACSL^{Phe}$ (Figure 3). This weakening may reflect altered alignment of the hydrogen bonds of these base pairs as the base of ψ_{32} is stabilized toward the major groove by the water-mediated N1H-phosphate hydrogen bond (Figure 7). A ψ_{32} H6-A_{31} H2 NOE is consistent with the major groove displacement of the ψ_{32} base. This NOE is not observed in the unmodified molecule (42) and is not typical of 5′-AU-3′ base stacking in helices with regular A-form geometry.

The 32–38 bp in tRNA

The nucleotide composition of residues 32 and 38 is not an equal distribution of the pyrimidine and purine bases. tRNA sequence data show that position 38 is often adenine (67%),

but a significant fraction (30%) of position 38 nt are pyrimidines (14). Residue 32 is almost exclusively occupied by a pyrimidine base (>97%) and is modified in approximately a third of sequenced tRNA molecules on either the base or ribose group. The most common base modification at position 32 is pseudouridine and although this base does not alter the overall structure of the $ACSL^{Phe}$ loop compared to uridine, it partially destabilizes the tri-loop conformation and increases the stem melting temperature by about 3.5°C. Other modifications at position 32 are frequently those that favor the C3′ endo conformation of the ribose, such as pyrimidine 2′-O-methyl and the pyrimidine C2-thiol (47), which may help to maintain the helical integrity of the stem of the anticodon arm (48). Whether these modifications can alter or stabilize anticodon loop conformations or function as pseudouridine primarily to stabilize the stem has not been investigated.

The geometry of the ψ_{32} base in solution is different from that observed for position 32 residues in crystal structures of tRNAs. The crystal structures of several tRNAs reveal a highly conserved structural motif, the bifurcated hydrogen bond, between residues 32 and 38 (49) (Figure 8). The bifurcated hydrogen bond frequently involves proton donation by an exocyclic NH_2 group and acceptance by the O2 of C_{32} or U_{32}. This hydrogen bond configuration imposes an underwinding of the helix geometry at the 32–38 base step. For *E.coli* $tRNA^{Phe}$, the configuration would correspond to hydrogen bonding between A_{38} $N6H_2$ and ψ_{32} O4 (adjacent to the C5-C1′ glycosidic bond). This base arrangement of ψ_{32} and A_{38} is isosteric with other 32–38 pairs, such as C_{32}–A_{38} and U_{32}–C_{38}, that adopt the bifurcated hydrogen bond (49) (Figure 8). Auffinger and Westhof (49) have proposed the geometry of nt 32 and 38 resulting from the bifurcated hydrogen bond creates a transition between the stem and loop in the anticodon arm and facilitates formation of the U-turn. Thus, the 32–38 interaction may allow an open conformation of the loop without distortion of the canonical A-form stem. The results of this study indicate that if the bifurcated hydrogen exists in solution and functions in U-turn stabilization, the ψ_{32} modification alone is not sufficient to organize this motif.

The crystal structure of fully modified Cys-$tRNA^{Cys}$ in complex with EF-Tu and GDPNP presents an alternative conformation for the ψ_{32}-A_{38} base pair. In this structure, the ψ_{32} base adopts the *syn* configuration about the glycosidic bond and does not form any interactions with A_{38} (17). This configuration of the base can accommodate the ψ_{32} water-mediated hydrogen bond to the phosphate backbone and thus should retain the stabilizing effect conferred by pseudouridine in the *anti* configuration. Notably though, the anticodon loop in this complex adopts the characteristic U-turn motif with stacking of the anticodon bases G, C, and A. The EF-Tu protein-binds at the acceptor stem and has no contacts in the region of the anticodon arm, but the G and C nucleotides of the anticodon form intermolecular base pairs within the unit cell of the crystal. The structure of this molecule is of particular interest since the anticodon arm of $tRNA^{Cys}$ contains the same nucleotide base modifications found in fully modified *E.coli* $tRNA^{Phe}$, specifically ψ_{32}, ψ_{39}, and $ms^2i^6A_{37}$. These additional modifications could affect the conformation of the ψ_{32} base, however, neither ψ_{39} nor i^6A_{37} alone are sufficient to induce the *syn* conformation of ψ_{32} in solution (J.Cabello and E.P.Nikonowicz, unpublished data).

Pseudouridylation within the anticodon arm of tRNA is important to the overall fitness of an organism and loss of this modification can lead to a spectrum of growth defects in bacteria and yeast (50–54). Disruption of the *truA* gene which catalyzes formation of ψ_{38}, ψ_{39}, and ψ_{40} decreases polypeptide chain elongation rates and reduces cell growth rate ~30% (1,55). A similar effect is observed for the *deg1* gene of yeast that catalyzes ψ_{38} and ψ_{39} formation (54,56). *E.coli* that contain a catalytically inactive *truB* gene which catalyzes formation of ψ_{55} exhibit no growth defects (52), even though ψ_{55} is universally conserved (14). Pseudouridylation at position 32 is intermediate in its physiological effects. Cells that lack RluA activity have near normal growth rates, but are strongly selected against when grown in competition with wild type cells (51). However, given that RluA modifies only six tRNA isoaccpetors, unlike TruA and TruB that modify their target sites in all tRNA molecules in *E.coli*, the physiological effects of its loss are remarkable and suggest a critical role of ψ_{32} in proper tRNA function. The specific translational defects associated with loss of ψ_{32} have not been determined, but studies of position 32 mutations in other tRNAs suggest translational fidelity and wobble base recognition are likely to be impaired (23–25,57). The studies presented here indicate that a primary role of ψ_{32} is the stabilization of the stem of the anticodon arm. Thus, ψ_{32} may serve as a buffer to preserve the stability and the architecture of the stem within the context of other loop-destabilizing nucleotide modifications (42) or after formation of the U-turn.

SUPPLEMENTARY DATA

Supplementary Data are available at NAR Online.

ACKNOWLEDGEMENTS

We thank M. Michnicka for preparation of the T7 RNA polymerase and isotopically labeled 5′-rNTPs. This work was supported by NSF grant MCB-0078501 and by a grant from the Robert A. Welch Foundation (C1277) to E.P.N. Funding to pay the Open Access publication charges for this article was provided by the Robert A. Welch Foundation.

Conflict of interest statement. None declared.

REFERENCES

1. Björk,G.R. (1995) Biosynthesis and function of modified nucleosides. In Söll,D. and RajBhandary,U.L. (eds), *tRNA Structure, Biosynthesis, and Function*. American Society for Microbiology Press, Washington, D.C. pp. 165–206.
2. Garcia,G.A. and Goodenough-Lashua,D.M. (1998) Mechanisms of modifying enzymes. In Grosjean,H. and Benne,R. (eds), *Modification and Editing of RNA: The Alteration of RNA Structure and Function*. ASM Press, Washington, D.C. pp. 135–168.
3. Winkler,M.E. (1998) Genetics and regulation of tRNA and rRNA modification. In Grosjean,H. and Benne,R. (eds), *Modification and Editing of RNA: The Alteration of RNA Structure and Function*. ASM Press, Washington, D.C. pp. 441–469.

4. Agris,P.F. (1996) The importance of being modified: roles of modified nucleosides and Mg^{2+} in RNA structure and function. *Prog. Nucleic Acid Res. Mol. Biol.*, **53**, 79–129.
5. Charette,M. and Gray,M.W. (2000) Pseudouridine in RNA: what, where, how, and why. *IUBMB Life*, **49**, 341–351.
6. Ofengand,J. (2002) Ribosomal RNA pseudouridines and pseudouridine synthases [Erratum (2002) *FEBS Lett.* **517**, 287.]. *FEBS Lett.*, **514**, 17–25.
7. Neumann,J.M., Bernassau,J.M., Gueron,M. and Tran-Dinh,S. (1980) Comparative conformations of uridine and pseudouridine and their derivatives. *Eur. J. Biochem.*, **108**, 457–463.
8. Davis,D.R. (1998) Biophysical and conformational properties of modified nucleosides in RNA (NMR Studies). In Grosjean,H. and Benne,R. (eds), *Modification and Editing of RNA*. ASM Press, Washington, D.C. pp. 85–101.
9. Davis,D.R. (1995) Stabilization of RNA stacking by pseudouridine. *Nucleic Acids Res.*, **23**, 5020–5026.
10. Roy,S., Papastavros,M.Z., Sanchez,V. and Redfield,A.G. (1984) Nitrogen-15-labeled yeast $tRNA^{Phe}$: double and two-dimensional heteronuclear NMR of guanosine and uracil ring NH groups. *Biochemistry*, **23**, 4395–4400.
11. Griffey,R.H., Davis,D., Yamaizumi,Z., Nishimura,S., Bax,A., Hawkins,B. and Poulter,C.D. (1985) ^{15}N-labeled *Escherichia coli* $tRNA_f^{Met}$, $tRNA^{Glu}$, $tRNA^{Tyr}$, and $tRNA^{Phe}$. Double resonance and two-dimensional NMR of N1-labeled pseudouridine. *J. Biol. Chem.*, **260**, 9734–9741.
12. Hruska,F.E., Grey,A.A. and Smith,I.C. (1970) A nuclear magnetic resonance study of the molecular conformation of β-pseudouridine in aqueous solution. *J. Am. Chem. Soc.*, **92**, 4088–4094.
13. Yarian,C.S., Basti,M.M., Cain,R.J., Ansari,G., Guenther,R.H., Sochacka,E., Czerwinska,G., Malkiewicz,A. and Agris,P.F. (1999) Structural and functional roles of the N1- and N3-protons of ψ at tRNA's position 39. *Nucleic Acids Res.*, **27**, 3543–3549.
14. Sprinzl,M., Horn,C., Brown,M., Loudovitch,A. and Steinberg,S. (1998) Compilation of tRNA sequences and sequences of tRNA genes. *Nucleic Acids Res.*, **26**, 148–153.
15. Robertus,J.D., Ladner,J.E., Finch,J.R., Rhodes,D., Brown,R.S., Clark,B.F. and Klug,A. (1974) Structure of yeast phenylalanine tRNA at 3 Å resolution. *Nature*, **250**, 546–551.
16. Kim,S.-H., Suddath,F.L., Quigley,G.J., McPherson,A., Sussman,J.L., Wang,A.H.J., Seeman,N.C. and Rich,A. (1974) Three-dimensional tertiary structure of yeast phenylalanine transfer RNA. *Science*, **185**, 435–440.
17. Nissoen,P., Thirup,S., Kjeldgaard,M. and Nyborg,J. (1999) The crystal structure of Cys-tRNA-EF-Tu-GDPNP reveals general and specific features in the ternary complex and in tRNA. *Structure*, **7**, 143–156.
18. Moras,D., Comarmond,M.B., Fischer,J., Weiss,R., Thierry,J.C., Ebel,J.P. and Giege,R. (1980) Crystal structure of yeast $tRNA^{Asp}$. *Nature*, **288**, 669–674.
19. Arnez,J.G. and Steitz,T.A. (1994) Crystal structure of unmodified $tRNA^{Gln}$ complexed with glutaminyl-tRNA synthetase and ATP suggests a possible role for pseudo-uridines in stabilization of RNA structure. *Biochemistry*, **33**, 7560–7567.
20. Shi,H. and Moore,P.B. (2000) The crystal structure of yeast phenylalanine tRNA at 1.93 Å resolution: a classic structure revisited. *RNA*, **6**, 1091–1105.
21. Westhof,E., Dumas,P. and Moras,D. (1985) Crystallographic refinement of yeast aspartic acid transfer RNA. *J. Mol. Biol.*, **184**, 119–145.
22. Yarus,M. (1982) Translational efficiency of transfer RNAs: uses of an extended anticodon. *Science*, **218**, 646–652.
23. Yarus,M., Cline,S., Raftery,L., Wier,P. and Bradley,D. (1986) The translational efficiency of tRNA is a property of the anticodon arm. *J. Biol. Chem.*, **261**, 10496–10505.
24. Lustig,F., Boren,T., Claesson,C., Simonsson,C., Barciszewska,M. and Lagerkvist,U. (1993) The nucleotide in position 32 of the tRNA anticodon loop determines ability of anticodon UCC to discriminate among glycine codons. *Proc. Natl Acad. Sci. USA*, **90**, 3343–3347.
25. Claesson,C., Lustig,F., Boren,T., Simonsson,C., Barciszewska,M. and Lagerkvist,U. (1995) Glycine codon discrimination and the nucleotide in position 32 of the anticodon loop. *J. Mol. Biol.*, **247**, 191–196.
26. O'Connor,M. (1998) tRNA imbalance promotes -1 frameshifting via near-cognate decoding. *J. Mol. Biol.*, **279**, 727–736.
27. Davanloo,P., Rosenberg,A.H., Dunn,J.J. and Sturdier,F.W. (1984) Cloning and expression of the gene for bacteriophage T7 RNA polymerase. *Proc. Natl Acad. Sci. USA*, **81**, 2035–2039.
28. Wrzesinski,J., Nurse,K., Bakin,A., Lane,B.G. and Ofengand,J. (1995) A dual-specificity pseudouridine synthase: an *Escherichia coli* synthase purified and cloned on the basis of its specificity for ψ_{746} in 23S RNA is also specific for ψ_{32} in $tRNA^{Phe}$. *RNA*, **4**, 437–448.
29. Nikonowicz,E.P., Sirr,A., Legault,P., Jucker,F.M., Baer,L.M. and Pardi,A. (1992) Preparation of ^{13}C and ^{15}N Labelled RNAs for heteronuclear multi-dimensional NMR studies. *Nucleic Acids Res.*, **20**, 4507–4513.
30. Markley,J.L., Bax,A., Arata,Y., Hilbers,C.W., Kaptein,R., Sykes,B.D., Wright,P.E. and Wuthrich,K. (1998) Recommendations for the presentation of NMR structures of proteins and nucleic acids. IUPAC-IUBMB-IUPAB Inter-Union Task Group on the Standardization of Data Bases of Protein and Nucleic Acid Structures Determined by NMR Spectroscopy. *J. Biomol. NMR*, **12**, 1–23.
31. Nikonowicz,E.P. and Pardi,A. (1993) An efficient procedure for assignment of the proton, carbon, and nitrogen resonances in ^{13}C/^{15}N labeled nucleic acids. *J. Mol. Biol.*, **232**, 1141–1156.
32. Legault,P., Farmer,B.T.II, Mueller,L. and Pardi,A. (1994) Through-bond correlation of adenine protons in a ^{13}C-labeled ribozyme. *J. Am. Chem. Soc.*, **116**, 2203–2204.
33. Hennig,M. and Williamson,J.R. (2000) Detection of N-H•••N hydrogen bonding in RNA via scalar couplings in the absence of observable imino proton resonances. *Nucleic Acids Res.*, **28**, 1585–1593.
34. Kellogg,G.W. and Schweitzer,B.I. (1993) Two- and three-dimensional ^{31}P-driven NMR procedures for complete assignment of backbone resonances in oligodeoxyribonucleotides. *J. Biomol. NMR*, **3**, 577–595.
35. Altona,C. (1982) Conformational analysis of nucleic acids. Determination of backbone geometry of single-helical RNA and DNA in aqueous solution. *Recl. Trav. Chim. Pays-Bas*, **101**, 413–433.
36. Smith,J.S. and Nikonowicz,E.P. (1998) NMR structure and dynamics of an RNA motif common to the spliceosome branch-point helix and the RNA-binding site for phage GA coat protein. *Biochemistry*, **37**, 13486–13498.
37. Varani,G., Aboul-ela,F. and Allain,F.H.-T. (1996) NMR investigation of RNA structure. *Prog. NMR Spectroscopy*, **29**, 51–127.
38. Gorenstein,D.G. (1981) Nucleotide conformational analysis by ^{31}P nuclear magnetic resonance spectroscopy. *Annu Rev Biophys Bioeng.*, **10**, 355–386.
39. Brünger,A.T. (1992) *X-PLOR Version 3.1 Manual*, Yale University, NH.
40. Pardi,A. (1995) Multidimensional heteronuclear NMR experiments for structure determination of isotopically labeled RNA. *Methods Enzymol.*, **261**, 350–380.
41. Sklenar,V., Peterson,R.D., Rejante,M.R. and Feigon,J. (1994) Correlation of nucleotide base and sugar protons in a ^{15}N-labeled HIV-1 RNA oligonucleotide by ^{1}H-^{15}N HSQC experiments. *J. Biomol. NMR*, **4**, 117–122.
42. Cabello-Villegas,J., Winkler,M.E. and Nikonowicz,E.P. (2002) Solution conformations of unmodified and $A_{37}N^6$-dimethylallyl modified anticodon stem–loops of *Escherichia coli* $tRNA^{Phe}$. *J. Mol. Biol.*, **319**, 1015–1034.
43. Hall,K.B. and McLaughlin,L.W. (1992) Properties of pseudouridine N1 imino protons located in the major groove of an A-form RNA duplex. *Nucleic Acids Res.*, **20**, 1883–1889.
44. Meroueh,M., Grohar,P.J., Qiu,J., SantaLucia,J.Jr, Scaringe,S.A. and Chow,C.S. (2000) Unique structural and stabilizing roles for the individual pseudouridine residues in the 1920 region of *Escherichia coli* 23S rRNA. *Nucleic Acids Res.*, **28**, 2075–2083.
45. Auffinger,P. and Westhof,E. (1997) RNA hydration: three nanoseconds of multiple molecular dynamics simulations of the solvated $tRNA^{Asp}$ anticodon hairpin. *J. Mol. Biol.*, **269**, 326–341.
46. Davis,D.R., Veltri,C.A. and Nielsen,L. (1998) An RNA model system for investigation of pseudouridine stabilization of the codon-anticodon interaction in $tRNA^{Lys}$, $tRNA^{His}$ and $tRNA^{Tyr}$. *J. Biomol. Struct. Dyn.*, **15**, 1121–1132.
47. Yokoyama,S. and Nishimura,S. (1995) Modified nucleosides and codon recognition. In Söll,D. and RajBhandary,U.L. (eds), *tRNA Structure, Biosynthesis, and Function.* American Society for Microbiology Press, Washington, D.C. pp. 207–224.
48. Kawai,G., Yamamoto,Y., Kamimura,T., Masegi,T., Sekine,M., Hata,T., Iimori,T., Watanabe,T., Miyazawa,T. and Yokoyama,S. (1992)

Conformational rigidity of specific pyrimidine residues in tRNA arises from posttranscriptional modifications that enhance steric interaction between the base and the 2′-hydroxyl group. *Biochemistry*, **31**, 1040–1046.
49. Auffinger,P. and Westhof,E. (1999) Singly and bifurcated hydrogen-bonded base-pairs in tRNA anticodon hairpins and ribozymes. *J. Mol. Biol.*, **292**, 467–483.
50. Tsui,H.C., Arps,P.J., Connolly,D.M. and Winkler,M.E. (1991) Absence of *hisT*-mediated tRNA pseudouridylation results in a uracil requirement that interferes with *Escherichia coli* K-12 cell division. *J Bacteriol*, **173**, 7395–7400.
51. Raychaudhuri,S., Niu,L., Conrad,J., Lane,B.G. and Ofengand,J. (1999) Functional effect of deletion and mutation of the *Escherichia coli* ribosomal RNA and tRNA pseudouridine synthase RluA. *J. Biol. Chem.*, **274**, 18880–18886.
52. Gutgsell,N., Englund,N., Niu,L., Kaya,Y., Lane,B.G. and Ofengand,J. (2000) Deletion of the *Escherichia coli* pseudouridine synthase gene *truB* blocks formation of pseudouridine 55 in tRNA *in vivo*, does not affect exponential growth, but confers a strong selective disadvantage in competition with wild-type cells. *RNA*, **6**, 1870–1881.
53. Del Campo,M., Kaya,Y. and Ofengand,J. (2001) Identification and site of action of the remaining four putative pseudouridine synthases in *Escherichia coli*. *RNA*, **7**, 1603–1615.
54. Lecointe,F., Simos,G., Sauer,A., Hurt,E.C., Motorin,Y. and Grosjean,H. (1998) Characterization of yeast protein Deg1 as pseudouridine synthase (Pus3) catalyzing the formation of Ψ_{38} and Ψ_{39} in tRNA anticodon loop. *J. Biol. Chem.*, **273**, 1316–1323.
55. Singer,C.E., Smith,G.R., Cortese,R. and Ames,B.N. (1972) Mutant $tRNA^{His}$ ineffective in repression and lacking two pseudouridine modifications. *Nature New Biol.*, **238**, 72–74.
56. Carbone,M.L., Solinas,M., Sora,S. and Panzeri,L. (1991) A gene tightly linked to CEN6 is important for growth of *Saccharomyces cerevisiae*. *Curr. Genet.*, **19**, 1–8.
57. Yarus,M., Cline,S.W., Wier,P., Breeden,L. and Thompson,R.C. (1986) Actions of the anticodon arm in translation on the phenotypes of RNA mutants. *J. Mol. Biol.*, **192**, 235–255.